Extracellular matrix protein tenascin C increases phagocytosis mediated by CD47 loss of function in glioblastoma

Ding Ma[1,2], **Senquan Liu**[3], **Bachchu Lal**[1,2], **Shuang Wei**[1,2], **Shuyan Wang**[1,2], **Daqian Zhan**[1,2], **Hao Zhang**[4], **Richard S. Lee**[5], **Peisong Gao**[6], **Hernando Lopez-Bertoni**[1,2], **Mingyao Ying**[1,2], **Jian Jian Li**[7], **John Laterra**[1,2,8,9], **Mary Ann Wilson**[1,2], **Shuli Xia**[1,2]

[1]Hugo W. Moser Research Institute at Kennedy Krieger, Baltimore, MD, 21205, USA

[2]Department of Neurology, Johns Hopkins School of Medicine, Baltimore, MD, 21205, USA

[3]Medicine, Johns Hopkins School of Medicine, Baltimore, MD, 21205, USA

[4]Molecular Microbiology and Immunology, Bloomberg School of Public Health, Johns Hopkins School of Medicine, Baltimore, MD, 21205, USA

[5]Psychiatry and Behavioral Sciences, Johns Hopkins School of Medicine, Baltimore, MD, 21205, USA

[6]Asthma and Allergy Center, Johns Hopkins School of Medicine, Baltimore, MD 21205, USA

[7]Department of Radiation Oncology, University of California Davis, Sacramento, CA, USA

[8]Department of Neurosurgery, Johns Hopkins School of Medicine, Baltimore, MD 21205, USA

[9]Oncology, Johns Hopkins School of Medicine, Baltimore, MD 21205, USA

Abstract

Glioblastomas (GBM) are highly infiltrated by myeloid-derived innate immune cells that contribute to the immunosuppressive nature of the brain tumor microenvironment (TME). CD47 has been shown to mediate immune evasion, as the CD47-SIRPα axis prevents phagocytosis of tumor cells by macrophages and other myeloid cells. In this study, we established CD47 homozygous deletion (CD47−/−) in human and mouse GBM cells and investigated the impact of eliminating the "don't eat me" signal on tumor growth and tumor-TME interactions. CD47 knockout (KO) did not significantly alter tumor cell proliferation in vitro but significantly increased phagocytosis of tumor cells by macrophages in co-cultures. Compared with CD47 wild type xenografts, orthotopic xenografts derived from CD47−/− tumor cells grew significantly slower with enhanced tumor cell phagocytosis and increased recruitment of M2-like tumor associated microglia/macrophages (TAM). CD47 KO increased tumor-associated extracellular matrix protein tenascin C (TNC) in xenografts, which was further examined in vitro. CD47 loss-of-function upregulated TNC expression in tumor cells via a Notch pathway-mediated mechanism.

§:**Corresponding Author** Dr. Shuli Xia, Hugo W. Moser Research Institute at Kennedy Krieger, Department of Neurology, Johns Hopkins School of Medicine, 707 N. Broadway, Room 400K, Baltimore, MD 21205, USA. Phone: 443-923-9498, Fax: 443-923-2695, xia@kennedykrieger.org.

Depletion of TNC in tumor cells enhanced the growth of CD47−/− xenografts in vivo and decreased the number of TAM. TNC knockdown also inhibited phagocytosis of CD47−/− tumor cells in co-cultures. Furthermore, TNC stimulated release of pro-inflammatory factors including TNF-α via a toll-like receptor 4 (TLR4) and STAT3-dependent mechanism in human macrophage cells. These results reveal a vital role for TNC in immunomodulation in brain tumor biology and demonstrate the prominence of the TME extracellular matrix in affecting the anti-tumor function of brain innate immune cells.

Keywords

CD47; Tenascin C; genome editing; phagocytosis; tumor-associated microglia/macrophages (TAMs); the tumor microenvironment; extracellular matrix; Iba-1; arginase-1

Introduction

Gliomas account for 70% of all adult brain tumors. Grade IV astrocytoma, glioblastoma (GBM) is the most common and aggressive primary brain tumor, accounting for approximately 50% of all glial tumor types. Because of tumor heterogeneity and the blood-brain barrier, GBM remains refractory to current treatment modalities including surgery, radiotherapy and chemotherapy; the median survival time of patients with GBM is ~15-20 months (1). Recent progress in immunotherapy-based treatment options in other tumor types has encouraged interest in developing similar approaches that might be effective for this devastating malignancy (2). However, current immunotherapies have not yet improved the survival of GBM patients (3). Understanding how tumor interacts with brain immune systems, including the innate immune system, and developing improved therapeutic options for GBM are urgently needed.

Innate immune cells, such as microglia, macrophages, and myeloid-derived suppressor cells, are known to be present within GBM. Tumor associated microglia/macrophages (TAMs) contribute to 30-50% of brain tumor mass (4, 5) and are educated by tumor cells to acquire a tumor-promoting M2-like phenotype that is able to produce anti-inflammatory and immune suppressive factors in the tumor microenvironment (TME). In GBMs, TAMs with different phenotypes co-exist, including an anti-tumor, pro-inflammatory M1-like phenotype. The activation status rather than the abundance of TAMs present in the TME has been shown to have prognostic value (6).

TME can influence the properties of TAMs (7). Extracellular matrix (ECM) is an important component of the TME and is composed of a complex mixture of macromolecules including glycoproteins, proteoglycans and polysaccharides. A body of evidence indicates that in addition to their canonical role in maintaining and regulating tissue organization, ECM components function as signaling molecules by interacting with membrane-bound receptors to regulate cell growth, motility and immune response (8). Although tightly controlled during embryonic development and organ homeostasis, these ECM-mediated pathways are commonly deregulated and disorganized in cancer. How ECM regulates immune response of brain tumors is largely unknown.

In this study, we used CD47 knockout (KO) human and mouse glioma models to investigate how ECM modulates the interactions between brain tumor cells and the innate immune system. CD47, also known as integrin-associated protein, is a ubiquitous 50 kDa membrane-bound protein consisting of a single N-terminal IgV extracellular domain, five membrane-spanning segments and a short C-terminal cytoplasmic tail (9). CD47 has been reported to mediate immune evasion by interacting with the signal regulatory protein-alpha (SIRPα) expressed on macrophages and other myeloid cells (10). CD47 binding to SIRPα causes phosphorylation of the SIRPα cytoplasmic immunoreceptor tyrosine-based inhibition motifs (ITIM), leading to the recruitment of Src homology 2 domain-containing tyrosine phosphatases, which prevents myosin-IIA accumulation at the phagocytic synapse and consequently inhibits phagocytosis (11). Thus, the CD47-SIRPα axis, also known as a "don't eat me" signal, functions as a negative checkpoint for innate immunity. CD47 expression is elevated in many cancers; TCGA data analysis indicated that high CD47 expression in GBM correlates with poor patient survival (12). Blocking the CD47/SIRPα interaction facilitates phagocytosis and inhibits tumor growth in many preclinical cancer models (12, 13); for example, the administration of anti-CD47 mAbs reduced tumor growth and prevented lung cancer progression (14).

Abundant evidence supports that the signaling functions of CD47 go well beyond this passive anti-phagocytic role, with CD47 acting as a sensor for cell–microenvironment signals. As an example, CD47 interacts with other signaling molecules including the matricellular glycoprotein thrombospondin-1 (TSP-1) (15, 16) to regulate various cellular functions including cell migration, axon extension, cytokine production, and T cell activation (17-19). Therefore, it is critical to dissect the signaling network of CD47 in tumor cells and tumor cell-immune cell interactions. The current study in GBM models is aimed to understand how TME influences host response to tumor cells carrying CD47 KO. We found that CD47 KO dramatically increased tumor-associated ECM protein tenascin C (TNC) *in vitro* and *in vivo*. Our results demonstrate the importance of the extracellular matrix protein in the anti-tumor function of brain innate immune cells.

Material and Methods

Reagents and Cell Cultures

All reagents were purchased from MilliporeSigma (Burlington, MA) unless otherwise stated. Human GBM cells U87, mouse glioma cells GL-261 and human monocyte cells THP-1 were original purchased from ATCC (Manassas, VA). All cell lines are free from mycoplasma and authenticated with short tandem repeat (STR) profiling by Johns Hopkins Genetic Resources Core facility using Promega GenePrint 10 system (Madison, WI).

Generation of CD47 KO cell lines by CRISPR-Cas9 system

Cas9-GFP plasmid was purchased from Addgene (Cambridge, MA). For targeting CD47, two gRNAs targeting CD47 were clone into pX330M (Addgene) according to the addgene cloning protocol. Human CD47 gRNA targeting sequences were: 5'-CGACCGCCGCCG CGCGTCACAGG (intron), and 5'-CAGCAACAGCGCCGCTACCAGGG (first exon). Mouse CD47 gRNA targeting sequences were: 5'- cccttgcatcgtccgtaatgtgg (intron), and 5'-

cagtagttttctttacgttaagg (first exon). Glioma cells (2×10^5 per well in 6-well plate) were co-transfected with the two gRNA plasmids and Cas9-GFP using lipofectamine 3000. After 2 days, transfected cells were sorted by flow cytometry (GFP[+]) and subcloned. Genomic DNA was extracted from clonal cells and amplified using the primer set as follows: for human: forward: 5'-GTCTGGAGCCTGCGACTG; reverse:5'-GTGTGTGCATTTGGAGATGG; for mouse: forward: 5'-gtctactggctggtgtgcaa; reverse:5'-catcgcgcttatccattttc. Sanger sequencing of the PCR products was performed to screen CD47 genomic KO.

Preparation of cell lines with TNC knockdown using shRNA and lentivirus system

To knock down TNC expression, lentivirus containing a control non-silencing (NS) sequence or TNC shRNA in a GIPZ viral vector (Thermo Fisher Scientific) containing the green fluorescent protein (GFP) coding frame was introduced into cells (20).

Cell migration assay

Migration was quantified by Boyden chamber transwell assays (8-mm pore size; Corning Costar) following our published work (21, 22).

Quantitative real-time PCR

Total RNA was extracted using RNeasy Mini Kit (Qiagen, Mansfield, MA). After reverse transcription using cDNA reverse transcriptase (Applied Biosystems, Calsbad, CA) and Oligo(dT) primer, quantitative real-time PCR (qRT-PCR) was performed using SYBR Green PCR Mix (Applied Biosystems) and IQ5 detection system (Bio-Rad, Hercules, CA). Primer sequences used in this study were listed in Supplemental Table 1. Relative gene expression was normalized to GAPDH.

Immunoblot

Proteins were detected and quantified using the Odyssey Infrared Imager (LI-COR Biosciences) with secondary antibodies labeled by IRDye infrared dyes (LI-COR Biosciences) and normalized to GAPDH or β-actin following our published work (20). The antibodies used for this study were listed below, most of them from Cell Signaling (Danvers, MA) unless otherwise stated: CD47 (Santa cruz, Dallas, TX); Tenascin C (mouse and human, MilliporeSigma); Tenascin C (human only, Santa cruz); STAT-3; phospho-STAT-3; Akt; phosphor-Akt; Jagged-1; NOTCH1; NICD; β-actin (MilliporeSigma); GAPDH (MilliporeSigma).

Enzyme-linked immunosorbent assay (ELISA) of TNF-a

Human monocyte cells THP-1 were seeded onto 12 well plates (1.5×10^5/well) and incubated with PMA (25 ng/ml) for 48 h to introduce differentiation. Cells were treated with tenascin C protein (TNC) at 1, 3, 10 μg/ml for another 8 h in serum free medium and the supernatant was collected for TNF-α measurement using a TNF-α ELISA kit (R&D systems, Minneapolis, MN). TNC was purchased from Millipore and purified from the conditioned medium of human U251 glioblastoma cell line by chromatography. All measurements were conducted according to the manufacturer's protocol using a microplate spectrophotometer (Molecular devices, San Jose, CA). For some experiments, cells were

incubated with STAT3 inhibitor (Stattic, 5 μmol/L) or TLR-4 inhibitor (TAK242, 10 μmol/L) for 1 h prior to TNC treatment.

In vitro phagocytosis assay

THP-1 cells were seeded onto 12 well plates (1.5×10^5/well) and incubated with PMA (25 ng/ml) for 48 h to induce differentiation. Cancer cells were labeled with CFSE (Thermo Fisher Scientific) following the manufacture's protocol. For each experiment, CFSE labeled tumor cells (3×10^5) were added to macrophages and incubated in a final volume of 1 ml serum-free medium at 37°C for 2 h. Macrophages were stained with CD11c-APC (Thermo Fisher Scientific) for 30 mins. Phagocytosis was assessed by flow cytometry (BD, Franklin Lakes, NJ). Non-stained and CD11c-APC-stained THP-1 cells were used for proper gating of flow cytometry analysis.

Tumor xenografts and immunofluorescent images

For intracranial xenografts, 8-week-old female severely immunodeficient mice (SCID) (NCI, Frederick, MD) received 100,000 viable CD47 WT or CD47$^{-/-}$ U87 cells in 2 μL of PBS by stereotactic injection into the right caudate/putamen. Mice were sacrificed ~3-4 weeks after implantation, tumor volumes were estimated based on the formula: vol = (sq. root of maximum cross-sectional area)^3 (23). All animal protocols used in this study were approved by the Johns Hopkins School of Medicine Animal Care and Use Committee.

Immunofluorescent staining of tumor sections was performed following the protocol in Wu et al (24). The primary antibodies used for immunofluorescent staining were as followings: Iba-1 (Wako, Thermofisher); iNOS (ThermoFisher); TGM2 (Cell signaling); Arginase-1(Cell signaling); Immunofluorescent images were taken under fluorescent microscopy and analyzed using Axiovision software (Zeiss, Germany). Fluorescent microphotographs were taken and positive staining were manually counted or quantified by ImageJ (NIH).

Statistical analysis

Statistical analysis was performed using Prism software (GraphPad, La Jolla, CA). Post hoc tests included the Students T-test and Tukey multiple comparison tests as appropriate. Data are represented as mean value ± standard error of mean (S.E.) and significance was set at $p < 0.05$.

Results

CD47 KO increases glioma cell phagocytosis

We employed the CRISPR-Cas9 technique to completely knockout *CD47* expression in human GBM cells to investigate the effect of CD47 loss-of-function on phagocytosis and tumor growth. Two guide RNAs (gRNA) separated by 108 bp and designed to target the first exon of *CD47* were transfected into U87 GBM cells (Fig. 1A). In all, ~20 clones were selected and analyzed via PCR for CD47 KO using a primer pair flanking the two gRNA target sites. Clones with heterozygous *CD47* deletion produced two PCR products of 588 bp and 480 bp; and homozygous deletion generated one 480 bp PCR product (Fig. 1B). Sanger

sequencing confirmed the homozygous deletion of the 108 bp targeted *CD47* genomic sequence in cells from clone 7 and clone 21 (CD47$^{-/-}$, Fig. 1C). Cell surface CD47 expression was absent in these two CD47$^{-/-}$ clonal lines as measured by both flow cytometry (Fig. 1D) and immunofluorescence (Fig. 1E).

Cell monolayer proliferation assays showed no significant difference in cell growth between CD47$^{-/-}$ cells and CD47 wild type control cells (WT) (Fig. 1F). Transwell migration assays revealed that CD47 knock out did not have a consistent effect on tumor cell migration, with clone 7 CD47 KO cells migrating slower than CD47 WT cells, but clone 21 similar to that of control (Fig. 1G).

Human monocyte cells THP-1 were differentiated into macrophages by phorbol 12-myristate 13-acetate (PMA, 25 ng/ml, 48-72 h) and used to evaluate the effect of CD47 KO on phagocytosis of U87 cell. CD47 WT and CD47$^{-/-}$ cells were labeled with carboxyfluorescein succinimidyl ester (CFSE), which covalently reacts with amine-containing residues of intracellular proteins. Labeled U87 cells were co-cultured with differentiated THP-1 cells for 2 h. The mixture were harvested and stained with the macrophage specific antibody CD11c conjugated with allophycocyanin (APC). Flow cytometry analysis was employed to detect CD11c$^+$/CFSE$^+$ macrophages, indicative of U87 phagocytosis. The phagocytosis index was calculated as the percentage of CD11c+ THP-1 cells that were also CFSE+ (red boxes in Fig. 1H, 1I). Co-culturing U87 WT cells with THP-1 cells revealed a baseline phagocytosis index of ~9.5%. CD47 KO increased the phagocytosis index by 3-4 fold to 39% and 31% in clones 7 and 21, respectively (Fig. 1I, n=6, *P*<0.001). This result is consistent with an anti-phagocytosis function of CD47 expression on tumor cells.

CD47 loss-of-function decreases GBM xenograft growth

We examined how CD47 KO affected GBM xenograft growth. U87 WT or CD47$^{-/-}$ cells (100,000) were separately injected into the caudate-putamen of Balb/c immunodeficient (SCID) mice (experiments were repeated once, n=8 total); animals were sacrificed ~4 weeks after implantation, and brain sections were stained with H&E (Fig. 2A). Control tumors were substantially larger with an average estimated volume of 40 mm^3 compared to xenografts from CD47$^{-/-}$ clones 21 and 7 that were ~5.7 mm^3 and 1.3 mm^3 after 4 weeks, respectively (Fig. 2B, *P*<0.001). CD47 expression was confirmed to be low in tumors derived from CD47$^{-/-}$ cells (Fig. 2C). The proliferation rate of tumor cells was examined by Ki67 staining and no significant difference between WT and CD47$^{-/-}$ tumors was found (48% vs. 40%, Fig. 2D, E). Closer examination of the xenografts revealed histopathological differences between the control and CD47$^{-/-}$ tumors. Control tumors displayed well-demarcated tumor margins as revealed by H&E staining (Fig. 2F, left panel), and immunofluorescence staining with an anti-human nuclear specific antigen antibody (Fig. 2G, left panel). In comparison, CD47$^{-/-}$ xenografts had very irregular margins (Fig. 2F **and** G, right panels). Furthermore, when similar-sized control and CD47$^{-/-}$ xenografts were compared, we found fewer blood vessels in CD47$^{-/-}$ xenografts (Fig. 2H, I, *P*<0.001), which may limit tumor growth. Immunohistochemical staining for cleaved caspase 3 revealed no differences in tumor cell apoptosis between control and CD47$^{-/-}$ xenografts (Supplemental

Fig. 1A, B). These findings, in conjunction with our results showing that CD47 KO minimally affected the growth rate and migration of U87 cells while increasing macrophage phagocytosis of tumor cell *in vitro*, led us to hypothesize that the substantial differences in WT and $CD47^{-/-}$ *in vivo* growth patterns resulted from differences in interactions between tumor cells and innate immune cells.

CD47 loss-of-function recruits more TAMs

The glioma-associated innate immune system, the main constitutes of which are tumor-associated microglia/ macrophages (TAMs), remain intact in SCID mice. We examined TAMs in CD47 WT and $CD47^{-/-}$ xenografts using specific markers. Immunofluorescence staining of the general microglial/macrophage marker Iba-1 revealed that consistent with reports from others (25), TAMs formed a dense band surrounding the WT tumors, and appeared sparsely within the tumors (Supplemental Fig. 2). The morphology of TAMs in the tumor core resembled amoeboid-like microglia/macrophages with stout processes (Fig. 3A, upper panels). In $CD47^{-/-}$ xenografts, the morphology of TAMs in the tumor core was similar to that of controls, but we observed an increase in the density of TAMs in CD47 KO xenografts (Fig. 3A, lower panels). The average number of Iba-1$^+$ cells per microscopic field was 105 in $CD47^{-/-}$ xenografts, almost 2 fold higher than that of control (Fig. 3B, $P<0.05$).

CD47 antibody has been shown to drive M2 to M1 polarization of macrophages *in vitro* (26). We asked if CD47 KO induces an increase in M1-like TAMs in GBM orthotopic xenografts. Expression of M1 marker iNOS (27) as well as M2 markers arginase 1 (Arg-1) (28) and transglutaminase 2 (Tgm2) (29) was examined by immunofluorescence to evaluate relative numbers of M1 and M2 macrophages in orthotopic WT and $CD47^{-/-}$ xenografts. We found very few cells expressing the M1 marker iNOS in the control and $CD47^{-/-}$ xenografts (Supplemental Fig. 3A). On the other hand, the xenografts were infiltrated with M2-like TAMs as evidenced by Arg-1, which co-stained with Iba-1 (Fig. 3C). The average number of Arg-1$^+$ TAMs per microscopic field was significantly increased by CD47 KO, from 22 in WT tumors to 48 in $CD47^{-/-}$ tumors (Fig. 3D, $P<0.05$). Another M2 marker TGM2 also increased by ~3 fold in $CD47^{-/-}$ xenografts (Supplemental Fig. 3B).

To determine if CD47 KO stimulated phagocytosis *in vivo*, we co-stained brain sections with Iba-1 (Fig. 3E, green) and human nuclear specific antigen (Fig. 3E, HuNu, red). Confocal microscopic analysis demonstrated the engulfment of tumor cells by microglia/macrophages (Fig. 3F, arrows). We counted total Iba-1$^+$ cells and cells double labeled with Iba-1 and HuNu. In $CD47^{-/-}$ xenografts, an average of ~5.1% Iba-1$^+$ cells were also positive for HuNu in the nuclei; in contrast, Iba-1 and HuNu double stained cells were rare in WT xenografts (Fig. 3G, $P<0.05$). This data suggested that CD47 KO inhibited tumor growth by promoting phagocytosis through the recruitment of M2-like TAMs.

CD47 KO upregulates tenascin C

Tenascin C (TNC) is a major extracellular matrix (ECM) molecule in glioma and influences parenchymal-tumor cell interactions (30). Immunofluorescence staining with an antibody recognizing both mouse and human TNC revealed a dramatic increase in TNC expression in $CD47^{-/-}$ xenografts (Fig. 4A). To determine the source of the increased TNC, we stained

tumor sections with a species-specific anti-human TNC antibody and found a significant increase in the expression of human TNC in CD47$^{-/-}$ xenografts as well (Fig. 4B, C, P<0.001). RT-PCR and Western blot analysis of TNC expression *in vitro* confirmed that CD47 KO upregulated TNC expression by ~2 fold at the mRNA level, and ~4-5 fold at the protein level (Fig. 4D, E, P<0.05).

Cell signaling pathways were examined to determine the molecular mechanism by which CD47 KO increased TNC expression in GBM cells. Western blot analysis was employed to screen alterations in AKT, MAPK, Notch and Wnt pathways. Several Notch pathway effectors, including Jagged-1, NOTCH1 and NICD, were increased 1.9-4.7 fold in CD47$^{-/-}$ cells in comparison to WT cells (Fig. 4F). Jagged-1 and NOTCH1 mRNA levels were also upregulated in CD47$^{-/-}$ cells (Fig. 4G). Treating cells with the specific Notch pathway inhibitor DAPT (N-[N-(3,5-Diflurophenaacetyl-L-alanyl)]-S-phenylglycine t-Butyl Ester) decreased TNC protein level in CD47$^{-/-}$ cells but not in WT cells (Fig. 4H), suggesting that Notch signaling was a driver of TNC upregulation in the CD47$^{-/-}$ cells.

TNC is also upregulated in mouse glioma cells with CD47 KO

To determine whether our major findings in SCID mice also applies to immunocompetent animal models, we knocked out *Cd47* in mouse glioma GL261 cells using genome editing and guide RNAs targeting mouse *Cd47* exon 2 (Supplemental Fig. 4A). After subcloning and genotyping, we obtained GL261 cells with CD47 KO. Shown in Supplemental Fig. 4B is the Sanger sequencing of the PCR product from genomic DNA of GL261 clone 29 with a deletion of 161 bp at the *Cd47* exon 2. Cell surface CD47 expression was absent in clone 29 as measured by flow cytometry (Fig. 5A). CD47 KO did not alter GL261 proliferation and migration. Phagocytosis analysis with THP-1 cells confirmed that CD47 KO increased the phagocytosis index by ~2 fold from 19% to 40.1% in mouse glioma cells (Fig. 5B, P<0.001). In immunocompetent syngeneic C57BL/6 mice, CD47 KO decreased xenografts growth from 97 mm^3 to 18 mm^3 (Fig. 5C, D, n=5, P<0.05). Similarly, control GL-261 tumors displayed well-demarcated tumor margins, whereas Cd47$^{-/-}$ tumors had irregular margins (Fig. 5E). Furthermore, immunostaining of TNC in GL261 intracranial tumors indicated TNC was upregulated in Cd47$^{-/-}$ tumors by nearly 3 fold (Fig. 5F, G, P<0.05), which was confirmed by Western blot analysis (3.5 fold) of GL261 cells *in vitro* (Fig. 5H). This confirms that our findings in human GBM cells and SCID mice can be replicated in other model systems.

TNC knockdown abrogates the anti-tumor effect of CD47 KO

We hypothesized that TNC upregulation contributed to tumor growth inhibition in CD47$^{-/-}$ tumors. To test this, TNC expression in U87 control and CD47$^{-/-}$ cells was knocked down using TNC shRNA since TNC was more prominently upregulated by CD47 loss-of-functions in U87 cells. TNC shRNA decreased TNC expression by ~80% in both CD47 WT and CD47$^{-/-}$ cells relative to control cells transduced with non-silencing shRNA (NS) (Fig. 6A), consistent with the efficiency previously described by us (20). TNC knockdown (KD) did not affect cell growth rate *in vitro* (Fig. 6B).

Orthotopic tumor xenografts from U87 CD47 WT and CD47$^{-/-}$ cells with or without TNCKD were used to investigate the role of TNC upregulation in the altered growth of CD47$^{-/-}$ xenografts. Animals were sacrificed around post-implantation day 18. H&E staining of brain sections revealed that TNCKD increased the size of CD47$^{-/-}$ xenografts from 11 mm^3 to 30 mm^3 (Fig. 6C, D, $P<0.05$). Knocking down TNC alone in CD47 WT tumor cells also increased tumor growth from 27 mm^3 to 101 mm^3 ($P<0.05$), consistent with our previous published work that TNC loss-of-function increased tumor growth (28). The size of CD47$^{-/-}$ + TNC KD xenografts was significantly smaller than that of CD47 WT + TNC KD, indicating CD47 knockout dramatically impairs tumor growth even when tenascin C was knocked down ($P<0.05$). Immunofluorescence staining confirmed TNC downregulation in xenografts derived from TNC shRNA transduced cells (Fig. 6E).

Anti-Iba-1 and anti-Arg-1 immunofluorescence was used to investigate how changes in microenvironmental TNC levels altered interactions between TAMs and tumor cells. TNCKD abrogated the increase in TAM recruitment induced by CD47 KO (Fig. 6F). The average number Iba-1$^+$ TAMs per microscopic field decreased from 106 in CD47$^{-/-}$ +NS xenografts to 60 in CD47$^{-/-}$ +TNCKD xenografts (Fig. 6G, $P<0.05$). The number of Arg-1$^+$ TAMs in CD47$^{-/-}$ xenografts, however, was not changed by TNCKD (Supplemental Fig. 5).

TNC modulates tumor cell-immune cell interactions

Our *in vivo* results support a mechanism by which microenvironmental TNC mediates anti-tumor responses to CD47 KO. As an extracellular protein involved in integrin binding and cytoskeleton regulation (31, 32), we hypothesized that this function of TNC reflected changes in tumor cell phagocytosis by TAMs. Indeed, we found TNCKD inhibited phagocytosis triggered by CD47 KO *in vitro* (Fig. 7A). As shown before, CD47 KO increased phagocytosis of control U87 cells by ~3-4 fold, from 15.2% to 49.1%. TNCKD significantly decreased phagocytosis induced by CD47 KO from 49.1% to 28% (Fig. 7B, $P<0.05$). We also noticed that compared with U87 CD47 WT cells, TNCKD decreased the baseline phagocytosis from 15.2% to 8.1%, which may partially explain the increased tumor size from CD47 WT +TNCKD cells. Our findings suggest that elevated expression of TNC in CD47$^{-/-}$ cells promoted phagocytosis; and TNC expression in tumor cells could contribute to baseline phagocytosis independent of CD47.

Since TNC is upregulated in response to inflammation (33), we hypothesized that TNC may elicit other immunomodulation functions to facilitate tumor cell-immune cell interactions. To this end, we studied TNC gain-of-function using exogenous TNC. THP-1 cells were treated with human TNC (1-10 μg/ml) for 8 h followed by RT-PCR to measure the expression level of several pro-inflammatory factors including IL-1β, IL-6 and TNF-α. Cells treated with lipopolysaccharides (LPS) were used as a positive control. Real-time quantitative RT-PCR revealed a concentration-dependent upregulation of these pro-inflammatory factors (Fig. 7C, $P<0.05$). ELISA of THP-1 conditioned medium revealed concentration-dependent increase in TNF-α production driven by TNC (Fig. 7D, $P<0.05$). We performed immunohistochemistry staining of TNF-α in CD47 WT +/− NS and CD47$^{-/-}$ +/− TNCKD xenografts. Consistent with our *in vitro* studies, our *in vivo* staining indicated that CD47 knockout increased TNF-α staining by 63%, which was reversed when TNC was

knocked down (Fig. 7E, F, P<0.05). This result indicated that TNC upregulation driven by CD47 KO is involved in the increased cytokine production.

STAT3 was activated in THP-1 cells following TNC treatment (Fig. 7G). The STAT3 specific inhibitor stattic (5 μmol/L) prevented STAT3 activation in TNC-treated THP-1 cells and inhibited TNF-α production induced by TNC (Fig. 7H, P<0.05). Pre-incubating THP-1 cells with the toll-like receptor 4 (TLR4) inhibitor TAK242 (10 μmol/L) also inhibited TNC-induced STAT3 activation and TNF-α production (Fig. 7I, J, P<0.05). Taken together, our results indicated that the extracellular matrix protein TNC activated STAT3 and induced the secretion of pro-inflammatory factors in macrophage cells, which may explain the systemically increased recruitment of TAMs in CD47$^{-/-}$ xenografts.

Discussion

In this work we established CD47 loss-of-function in GBM cells to investigate the impact of eliminating the "don't eat me" signal on tumor growth and tumor-TME interactions. CD47 KO significantly decreased intracranial tumor growth by recruiting more M2-like TAMs and inducing phagocytosis. We found that CD47 KO in glioma cells upregulated the ECM protein TNC *in vitro* and in both SCID mice and immunocompetent mice. Knocking down TNC expression in tumor cells reversed CD47 KO-mediated phagocytosis *in vitro* and its anti-tumor effect *in vivo*. We also found TNC may elicit a systematic immunomodulation role via binding to TLR4 in macrophages to activate STAT3 and stimulate release of pro-inflammatory factors including TNF- α. To the best of our knowledge, this is the first study to link TNC to CD47-mediated phagocytosis signaling and demonstrate the importance of TNC in affecting the anti-tumor function of brain TAMs.

Our *in vitro* and *in vivo* phagocytosis analyses of CD47 KO cells are consistent with previous studies by others demonstrating that targeting the CD47-SIRPα axis with specific blocking antibody increases phagocytosis (12-14). CD47 is a multi-faceted molecule that interacts with many receptors/ligands to mediate a variety of biological functions. Our data suggest that apart from the "don't eat me" signaling pathway, CD47 KO also affects other pathways and molecules. It has been reported that CD47 serves as the receptor for matricellular protein thrombospondin-1 (TSP-1), a prototype of the matricellular protein family with members like TNC and secreted protein acidic and rich in cysteine (SPARC). TSP-1 is implicated in angiogenesis, which may explain changes in laminin staining observed in CD47$^{-/-}$ xenografts. Our data also found that TNC was upregulated by CD47 KO via a Notch mediated mechanism, consistent with report from Sivasankaran et al that the activation of the Notch pathway increased TNC expression (34). Kaur et al reported that CD47 knockdown leads to c-Myc activation and stem cell marker expression such as KLF4, OCT 4 and Sox2 (16). In GBM, the Notch pathway has been implicated in GBM stem cell biology (35). Therefore, it is tempting to speculate that CD47 KO upregulates the Notch pathway via alteration in stem cell related pathways. On the other hand, studies from Sarkar et al indicated Notch activation is downstream of TNC signaling in brain tumor stem cells (36). A detailed link between CD47 KO and TNC is currently under investigation.

In immunodeficient mice (SCID), the adaptive immune system, including T cells and B cells, is deficient; whereas the innate immune system, including microglia, macrophage, and natural killer cells, remains intact (37). The size of CD47$^{-/-}$ xenografts was much smaller compared with that of control, yet the number of infiltrating TAMs in CD47$^{-/-}$ xenografts was significantly higher than that of control. We reasoned that phagocytosis/cytotoxicity mediated by TAMs was the main contributor of the decreased tumor size in CD47$^{-/-}$ xenografts, because our *in vitro* analysis showed no growth difference between CD47 WT cells and CD47$^{-/-}$ cells. Our *in vivo* Ki67 staining further confirmed this. Thus, depending on the TME, high TAM density was not always associated with more aggressive tumors. Works from Loane et al. (38) indicated that TAMs with amoeboid-like shape were motile while the hypertrophic morphology of TAMs was associated with a phagocytic activity. In our models, the morphology of TAMs in CD47$^{-/-}$ xenografts was similar to that of controls with amoeboid-like shape. The increased density of Arg1+ in CD47$^{-/-}$ xenografts suggested that more M2-like TAMs were recruited by CD47 KO xenografts. Although Zhang et al reported that anti-CD47 antibody repolarized M2 macrophage to M1 macrophage (26), we did not observe such repolarization of TAMs following CD47 KO in our models. However, we were able to demonstrate the increased phagocytosis ability of TAMs in CD47$^{-/-}$ xenografts by double staining of human nuclei and Iba-1 in TAMs, consistent with studies for Leidi et al demonstrating that M2-like TAMs also have phagocytic ability (39).

Compared with U87 wild type xenografts that always form ball-like solid tumors, the histopathological features of CD47 KO xenografts show invasive margin of xenografts. This could either from the increased phagocytosis by infiltrating microglia/macrophages or increased tumor cell migratory due to high TNC level. Since the effect of CD47 KO on tumor cell migration was not consistent in different clones, we reason the increased phagocytosis may be the main cause for the dramatic change in the histopathological features of CD47 KO xenografts.

One of the interesting findings in this study is to link TNC as a modulator of phagocytosis in brain cancer. Our findings are in line with works regarding TNC function in the periphery system (40, 41). TNC is one of the most abundant ECM proteins in the brain TME and its expression correlates with GBM progression. Our findings that TNC was upregulated following CD47 KO and play a beneficial role to facilitate phagocytosis is counter-intuitive but not surprising as we have previously reported that targeting TNC in GBM stem-like neurosphere cells inhibited tumor migration but promoted tumor growth *in vivo* (20). As a consequence of its complex structure, TNC functions as an ECM molecule to activate the integrin signaling pathway during adhesion, migration and cytoskeleton rearrangement, which may also contribute to increased phagocytosis in CD47$^{-/-}$ xenografts as the phagocytosis process employs cytoskeleton such as myosin to form phagocytosis cup. Besides this, we also found that TNC may elicit a systematic role to facilitate phagocytosis by inducing pro-inflammatory factors, which may recruit more immune cells to attack tumor cells. It has been well-documented that TNC is upregulated during inflammation and plays an important role in wound healing (42, 43). In arthritic joint diseases, TNC has been reported to function as an endogenous activator of toll-like receptor 4 (TLR4) via its fibrogenin domain to induce inflammation (43). Our results of TNC function in brain tumor are consistent with the function of TNC in the periphery system. With the findings that TNC

is dramatically upregulated in CD47$^{-/-}$ xenografts and modulates phagocytosis, it is appealing to think that instead of being a promoter of tumor malignancy, the elevated TNC in brain tumors may be a defensive mechanism by the innate system to try to eliminate malignant cells.

Over the past years, the use of immune checkpoint inhibitors to target the adaptive immune systems has been one of the most significant advances in anti-tumor treatment. However, the increased use of these agents has led to an augmented appreciation that they were not suitable for all patients. Recent studies have indicated that the innate immune system checkpoint such as CD47 may be an interesting therapeutic target (44). A better mechanistic understanding of CD47 signaling network will aid in the development of novel anti-tumor reagent. Our study provides the first evidence demonstrating that microenvironmental TNC is involved in phagocytosis of tumor cell by TAMs. Future studies of the precise mechanism by which TNC regulates phagocytosis will shed light on how to exploit the innate immune system to target brain tumors.

Supplementary Material

Refer to Web version on PubMed Central for supplementary material.

Acknowledgements

References

1. Thomas AA, Brennan CW, DeAngelis LM, et al. Emerging therapies for glioblastoma. JAMA Neurol, 2014;71:1437–1444. [PubMed: 25244650]

2. Lim M, Xia Y, Bettegowda C, et al. Current state of immunotherapy for glioblastoma. Nat Rev Clin Oncol, 2018;15:422–442. [PubMed: 29643471]

3. Huang J, Liu F, Liu Z, et al. Immune Checkpoint in Glioblastoma: Promising and Challenging. Front Pharmacol, 2017;8:242. [PubMed: 28536525]

4. Quail DF, and Joyce JA The Microenvironmental Landscape of Brain Tumors. Cancer Cell, 2017;31:326–341. [PubMed: 28292436]

5. Hambardzumyan D, Gutmann DH, and Kettenmann H The role of microglia and macrophages in glioma maintenance and progression. Nat Neurosci, 2016;19:20–27. [PubMed: 26713745]

6. Poon CC, Sarkar S, Yong VW, et al. Glioblastoma-associated microglia and macrophages: targets for therapies to improve prognosis. Brain, 2017;140:1548–1560. [PubMed: 28334886]

7. Netea-Maier RT, Smit JWA, and Netea MG Metabolic changes in tumor cells and tumor-associated macrophages: A mutual relationship. Cancer Lett, 2018;413:102–109. [PubMed: 29111350]

8. Lu P, Weaver VM, and Werb Z The extracellular matrix: a dynamic niche in cancer progression. J Cell Biol, 2012;196:395–406. [PubMed: 22351925]

9. Sick E, Jeanne A, Schneider C, et al. CD47 update: a multifaceted actor in the tumour microenvironment of potential therapeutic interest. Br J Pharmacol, 2012;167:1415–1430. [PubMed: 22774848]

10. Veillette A, and Chen J SIRPalpha-CD47 Immune Checkpoint Blockade in Anticancer Therapy. Trends Immunol, 2018;39:173–184. [PubMed: 29336991]

11. Liu X, Kwon H, Li Z, et al. Is CD47 an innate immune checkpoint for tumor evasion? J Hematol Oncol, 2017;10:12. [PubMed: 28077173]

12. Willingham SB, Volkmer JP, Gentles AJ, et al. The CD47-signal regulatory protein alpha (SIRPa) interaction is a therapeutic target for human solid tumors. Proc Natl Acad Sci U S A, 2012;109:6662–6667. [PubMed: 22451913]

13. Zhao CL, Yu S, Wang SH, et al. Characterization of cluster of differentiation 47 expression and its potential as a therapeutic target in esophageal squamous cell cancer. Oncol Lett, 2018;15:2017–2023. [PubMed: 29399202]

14. Weiskopf K, Jahchan NS, Schnorr PJ, et al. CD47-blocking immunotherapies stimulate macrophage-mediated destruction of small-cell lung cancer. J Clin Invest, 2016;126:2610–2620. [PubMed: 27294525]

15. Gao Q, Chen K, Gao L, et al. Thrombospondin-1 signaling through CD47 inhibits cell cycle progression and induces senescence in endothelial cells. Cell Death Dis, 2016;7:e2368. [PubMed: 27607583]

16. Kaur S, Soto-Pantoja DR, Stein EV, et al. Thrombospondin-1 signaling through CD47 inhibits self-renewal by regulating c-Myc and other stem cell transcription factors. Sci Rep, 2013;3:1673. [PubMed: 23591719]

17. Bian Z, Shi L, Guo YL, et al. Cd47-Sirpalpha interaction and IL-10 constrain inflammation-induced macrophage phagocytosis of healthy self-cells. Proc Natl Acad Sci U S A, 2016;113:E5434–5443. [PubMed: 27578867]

18. Soto-Pantoja DR, Terabe M, Ghosh A, et al. CD47 in the tumor microenvironment limits cooperation between antitumor T-cell immunity and radiotherapy. Cancer Res, 2014;74:6771–6783. [PubMed: 25297630]

19. Zhao H, Wang J, Kong X, et al. CD47 Promotes Tumor Invasion and Metastasis in Non-small Cell Lung Cancer. Sci Rep, 2016;6:29719. [PubMed: 27411490]

20. Xia S, Lal B, Tung B, et al. Tumor microenvironment tenascin-C promotes glioblastoma invasion and negatively regulates tumor proliferation. Neuro Oncol, 2016;18:507–517. [PubMed: 26320116]

21. Oyinlade O, Wei S, Lal B, et al. Targeting UDP-alpha-D-glucose 6-dehydrogenase inhibits glioblastoma growth and migration. Oncogene, 2018;37:2615–2629. [PubMed: 29479058]

22. Wan J, Su Y, Song Q, et al. Methylated cis-regulatory elements mediate KLF4-dependent gene transactivation and cell migration. Elife, 2017;6.

23. Sun P, Xia S, Lal B, et al. Lipid metabolism enzyme ACSVL3 supports glioblastoma stem cell maintenance and tumorigenicity. BMC Cancer, 2014;14:401. [PubMed: 24893952]

24. Wu Y, Richard JP, Wang SD, et al. Regulation of glioblastoma multiforme stem-like cells by inhibitor of DNA binding proteins and oligodendroglial lineage-associated transcription factors. Cancer Sci, 2012;103:1028–1037. [PubMed: 22380883]

25. Gabrusiewicz K, Ellert-Miklaszewska A, Lipko M, et al. Characteristics of the alternative phenotype of microglia/macrophages and its modulation in experimental gliomas. PLoS One, 2011;6:e23902. [PubMed: 21901144]

26. Zhang M, Hutter G, Kahn SA, et al. Anti-CD47 Treatment Stimulates Phagocytosis of Glioblastoma by M1 and M2 Polarized Macrophages and Promotes M1 Polarized Macrophages In Vivo. PLoS One, 2016;11:e0153550. [PubMed: 27092773]

27. Bertolini TB, de Souza AI, Gembre AF, et al. Genetic background affects the expansion of macrophage subsets in the lungs of Mycobacterium tuberculosis-infected hosts. Immunology, 2016;148:102–113. [PubMed: 26840507]

28. Roszer T Understanding the Mysterious M2 Macrophage through Activation Markers and Effector Mechanisms. Mediators Inflamm, 2015;2015:816460. [PubMed: 26089604]

29. Martinez FO, Helming L, Milde R, et al. Genetic programs expressed in resting and IL-4 alternatively activated mouse and human macrophages: similarities and differences. Blood, 2013;121:e57–69. [PubMed: 23293084]

30. Midwood KS, Chiquet M, Tucker RP, et al. Tenascin-C at a glance. J Cell Sci, 2016;129:4321–4327. [PubMed: 27875272]

31. Yoshida T, Akatsuka T, and Imanaka-Yoshida K Tenascin-C and integrins in cancer. Cell Adh Migr, 2015;9:96–104. [PubMed: 25793576]

32. Fischer D, Tucker RP, Chiquet-Ehrismann R, et al. Cell-adhesive responses to tenascin-C splice variants involve formation of fascin microspikes. Mol Biol Cell, 1997;8:2055–2075. [PubMed: 9348542]

33. Midwood KS, and Orend G The role of tenascin-C in tissue injury and tumorigenesis. J Cell Commun Signal, 2009;3:287–310. [PubMed: 19838819]

34. Sivasankaran B, Degen M, Ghaffari A, et al. Tenascin-C is a novel RBPJkappa-induced target gene for Notch signaling in gliomas. Cancer Res, 2009;69:458–465. [PubMed: 19147558]

35. Hovinga KE, Shimizu F, Wang R, et al. Inhibition of notch signaling in glioblastoma targets cancer stem cells via an endothelial cell intermediate. Stem Cells, 2010;28:1019–1029. [PubMed: 20506127]

36. Sarkar S, Mirzaei R, Zemp FJ, et al. Activation of NOTCH Signaling by Tenascin-C Promotes Growth of Human Brain Tumor-Initiating Cells. Cancer Res, 2017;77:3231–3243. [PubMed: 28416488]

37. Arnold L, Tyagi RK, Mejia P, et al. Analysis of innate defences against Plasmodium falciparum in immunodeficient mice. Malar J, 2010;9:197. [PubMed: 20618960]

38. Loane DJ, Kumar A, Stoica BA, et al. Progressive neurodegeneration after experimental brain trauma: association with chronic microglial activation. J Neuropathol Exp Neurol, 2014;73:14–29. [PubMed: 24335533]

39. Leidi M, Gotti E, Bologna L, et al. M2 macrophages phagocytose rituximab-opsonized leukemic targets more efficiently than m1 cells in vitro. J Immunol, 2009;182:4415–4422. [PubMed: 19299742]

40. Marzeda AM, and Midwood KS Internal Affairs: Tenascin-C as a Clinically Relevant, Endogenous Driver of Innate Immunity. J Histochem Cytochem, 2018;66:289–304. [PubMed: 29385356]

41. Piccinini AM, and Midwood KS Endogenous control of immunity against infection: tenascin-C regulates TLR4-mediated inflammation via microRNA-155. Cell Rep, 2012;2:914–926. [PubMed: 23084751]

42. Jones FS, and Jones PL The tenascin family of ECM glycoproteins: structure, function, and regulation during embryonic development and tissue remodeling. Dev Dyn, 2000;218:235–259. [PubMed: 10842355]

43. Midwood K, Sacre S, Piccinini AM, et al. Tenascin-C is an endogenous activator of Toll-like receptor 4 that is essential for maintaining inflammation in arthritic joint disease. Nat Med, 2009;15:774–780. [PubMed: 19561617]

44. Weiskopf K Cancer immunotherapy targeting the CD47/SIRPalpha axis. Eur J Cancer, 2017;76:100–109. [PubMed: 28286286]

Significance: Findings link TNC to CD47-driven phagocytosis and demonstrate that TNC affects the anti-tumor function of brain TAM, facilitating the development of novel innate immune system-based therapies for brain tumors.
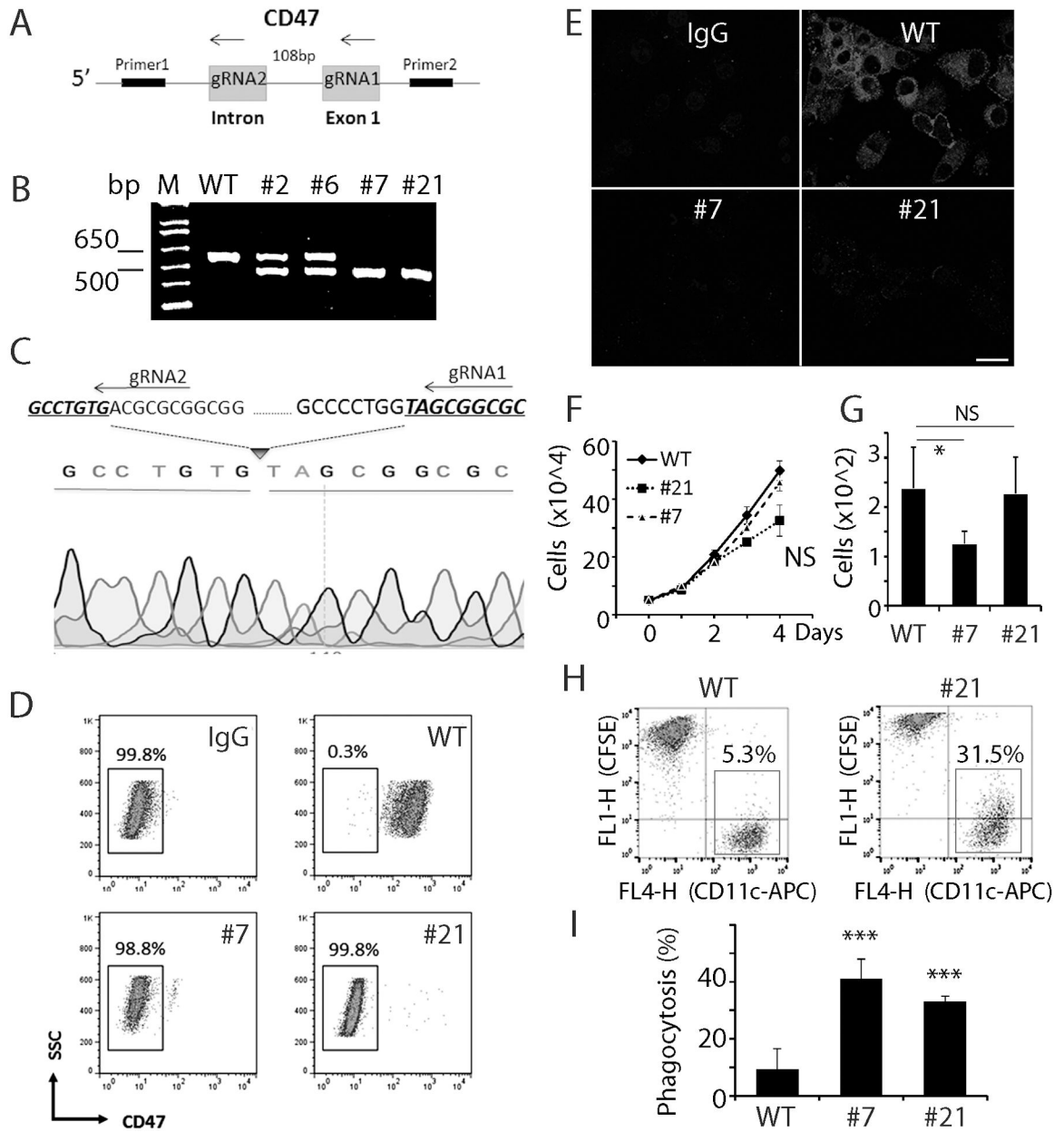
Fig. 1. Establish CD47 KO human GBM cells by genome editing.
A. Schematic graph of genome editing strategy with two guide RNAs to knockout CD47. **B.** PCR product from genomic DNA of selected clones showing heterozygous and homozygous deletion of CD47. **C.** Sanger sequencing of clone 21 showing deletion of part of the CD47 coding sequence. **D.** Flow cytometry analysis with a CD47 antibody indicated no CD47 expression on cell membrane in CD47$^{-/-}$ cells. Representative data of three measurements. **E.** Immunocytostaining of CD47 in control and CD47$^{-/-}$ cells. Bar = 20 μm. **F,** CD47 KO minimally affected cell proliferation *in vitro*. **G.** CD47 KO decreased cell migration of clone 7, but had no effect on clone 21 (G), n=3. **H.** Phagocytosis analysis of THP-1 cells cocultured with control and CD47$^{-/-}$ cells. **I.** Quantification of phagocytosis rate of THP-1 cells against CD47 WT and CD47$^{-/-}$ tumor cells. *: $P<0.05$, ***: $P<0.001$, n=6.
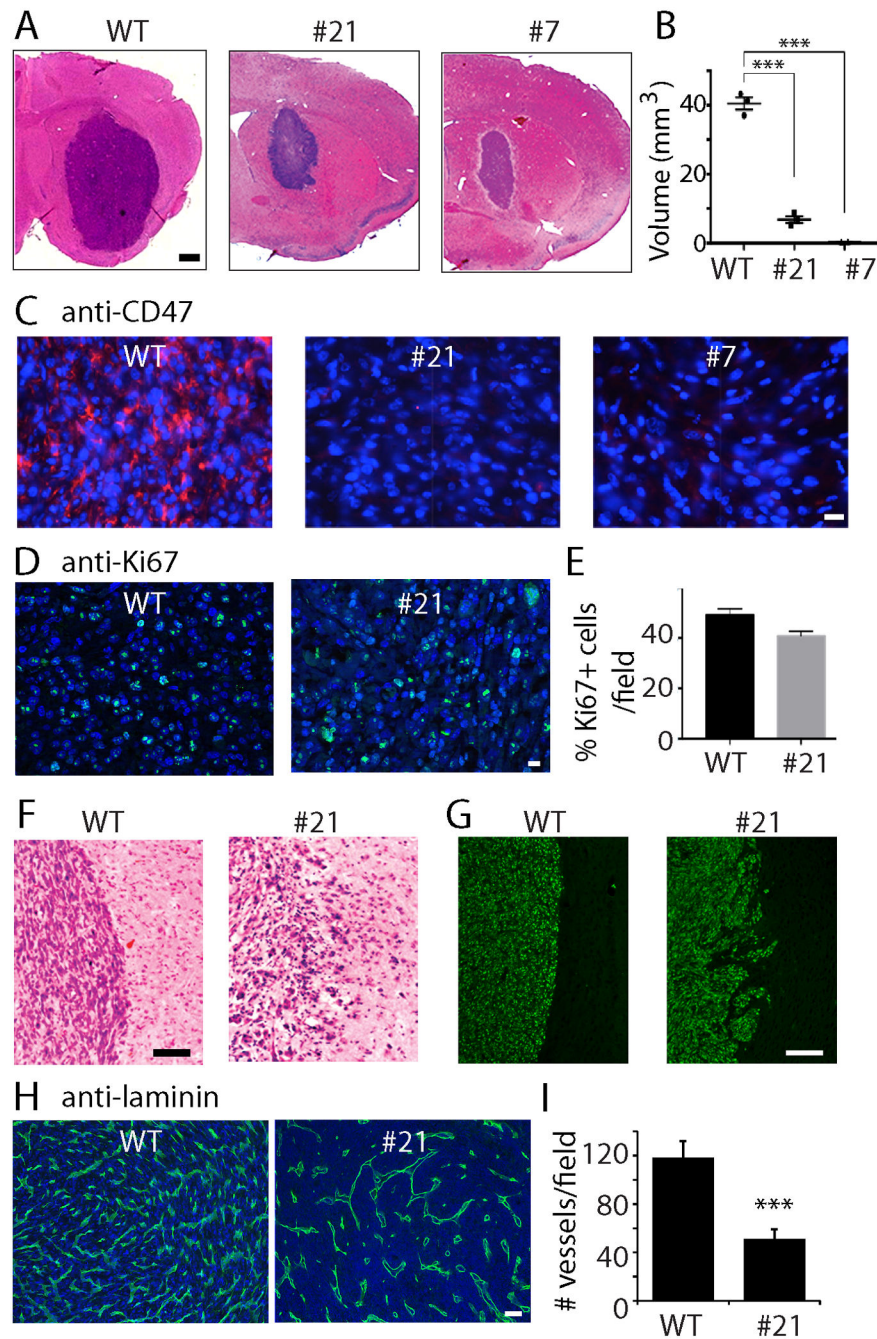
Fig. 2. Effect of CD47 KO on tumor growth.
A. Representative H &E staining of xenografts derived from control and CD47$^{-/-}$ cells. Bar = 500 μm. **B.** Quantification of the size of WT and CD47$^{-/-}$ xenografts. **C.** Immunofluorescent staining confirmed that CD47 expression was eliminated in CD47$^{-/-}$ xenografs. Bar = 20 μm. **D. E.** Ki67 staining and quantification in WT and CD47$^{-/-}$ xenografts. Bar = 20 μm. **F.** Representative microphotographs of H& E staining of well-demarcated margins in WT tumors (left) and irregular CD47$^{-/-}$ tumor margins (right). Bar = 100 μm. **G.** Xenografts were immunostained with an antibody against human nuclear

specific antigen to show tumor margins. Bar = 200 μm. **H, I.** Laminin staining to show blood vessels in control and CD47$^{-/-}$ xenografts. Bar = 100 μm. ***: P<0.001. In vivo experiments were repeated once. N=8 in total.
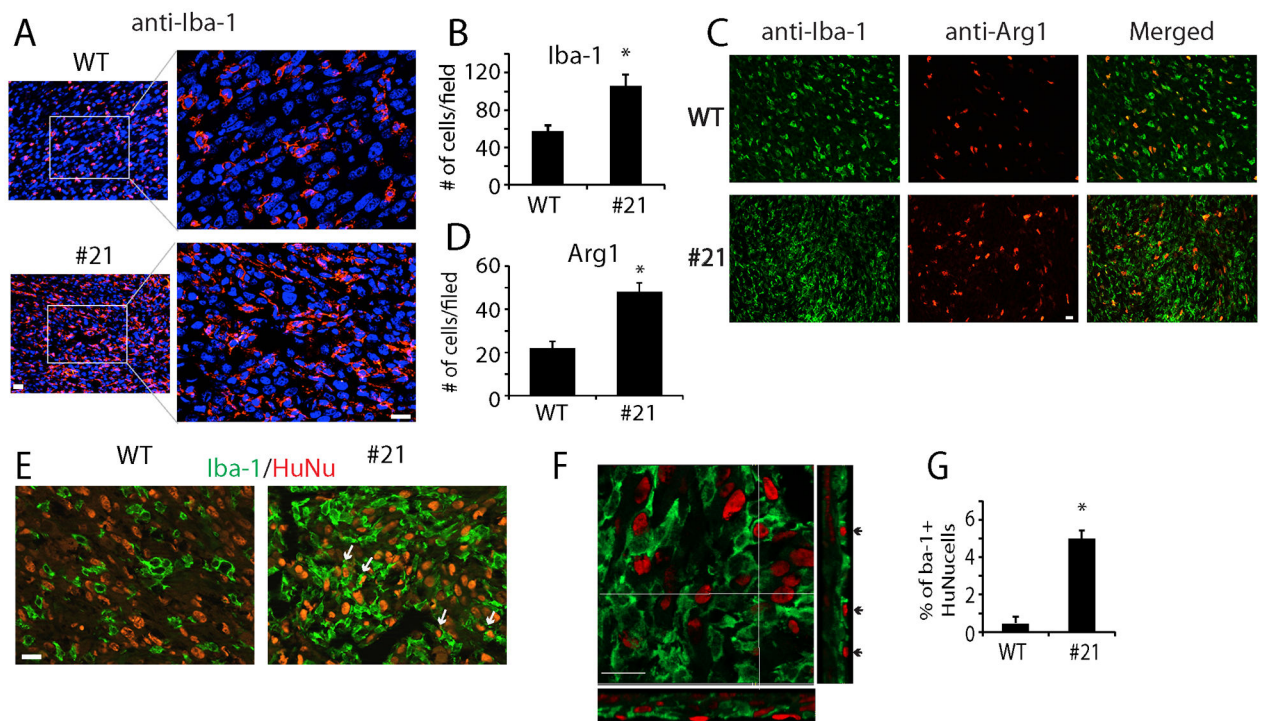
Fig. 3. Distribution of TAMs in xenografts.

A. Microglial/macrophage marker Iba-1 staining indicated higher density of TAMs in CD47$^{-/-}$ xenografts. **B.** Quantification of Iba$^+$ cells per microscopic field in control and CD47$^{-/-}$ xenografts. **C, D.** Co-staining of the M2 marker Arg-1 (red) and Iba-1 (green) in xenografts and quantification of Arg-1+ cells per field. **E.** Double-staining of TAMs (Iba-1$^+$, green) and tumor cells (HuNu$^+$, red) showing host immune cells with human tumor nuclei (Arrows) in CD47$^{-/-}$ xenografts. **F.** Confocal microscopic imaging of the double staining of Iba-1 and HuNu in a CD47$^{-/-}$ xenograft showing the two markers were from the same cells (Arrows). **G.** Quantification of Iba-1$^+$ cells with HuNu$^+$ staining per microscopic field. *: $P<0.05$, n=8. Bar = 20 μm.
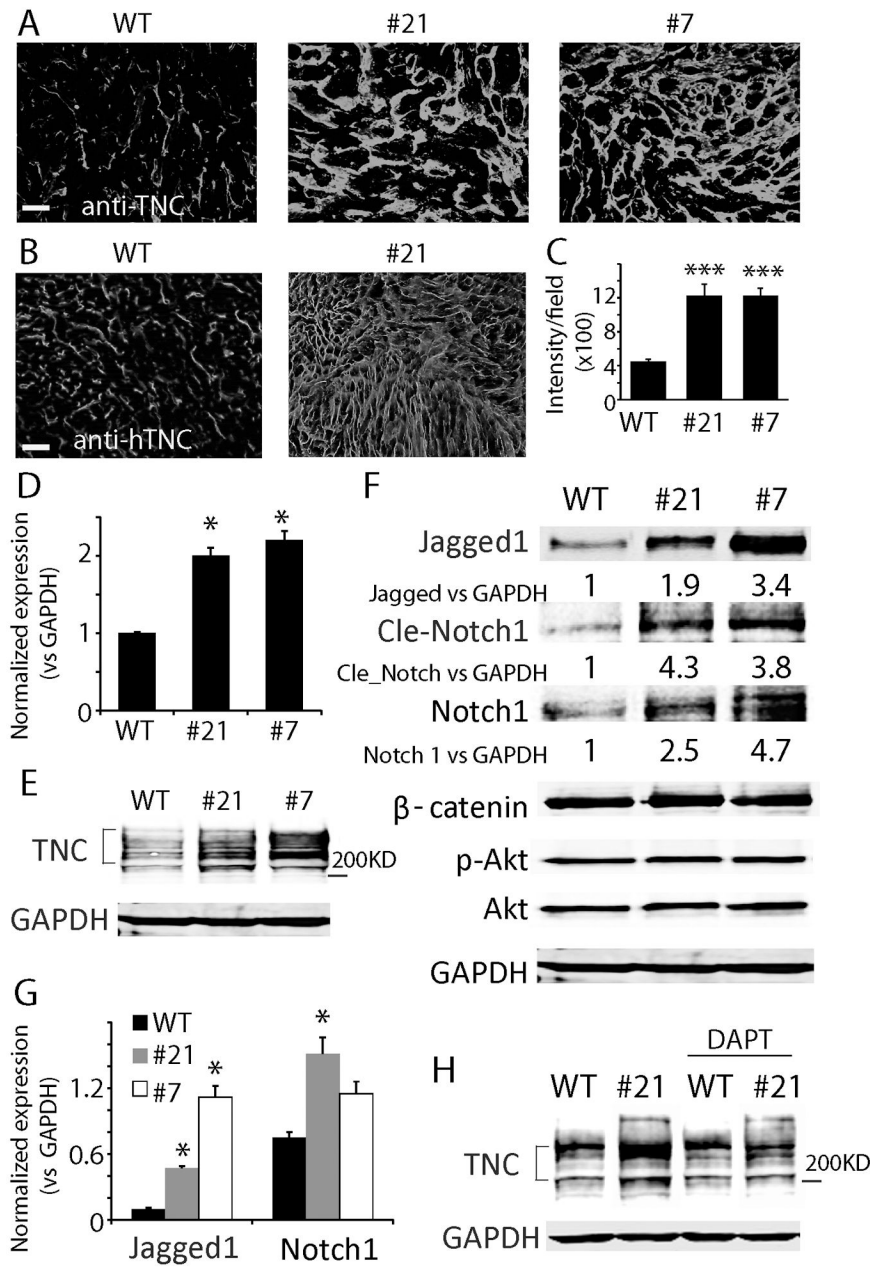
Fig. 4. Tenascin C (TNC) was upregulate in CD47$^{-/-}$ xenografts.
A. Immunofluorescence staining of TNC with an antibody recognizing both mouse and human TNC. **B.** Staining of TNC using an antibody that only recognizes human TNC. Bar = 100 μm. **C.** Quantification of human TNC staining intensity. **D, E.** RT-PCR and Western blot analysis confirmed TNC was upregulated at the mRNA and protein level (Mw 200-250 KD) in CD47$^{-/-}$ clonal cells. **F.** Signaling pathways activated in CD47$^{-/-}$ clones. The Notch but not Wnt and AKT pathways were elevated in CD47$^{-/-}$ cells. **G.** Jagged-1 and NOTCH1 were upregulated by CD47 KO at the mRNA level. **H.** Notch pathway inhibitor DAPT blunted TNC upregulation in CD47$^{-/-}$ cells. In vitro experiments were replicated at least three times. *: $P<0.05$, ***: $P<0.001$, n=8.
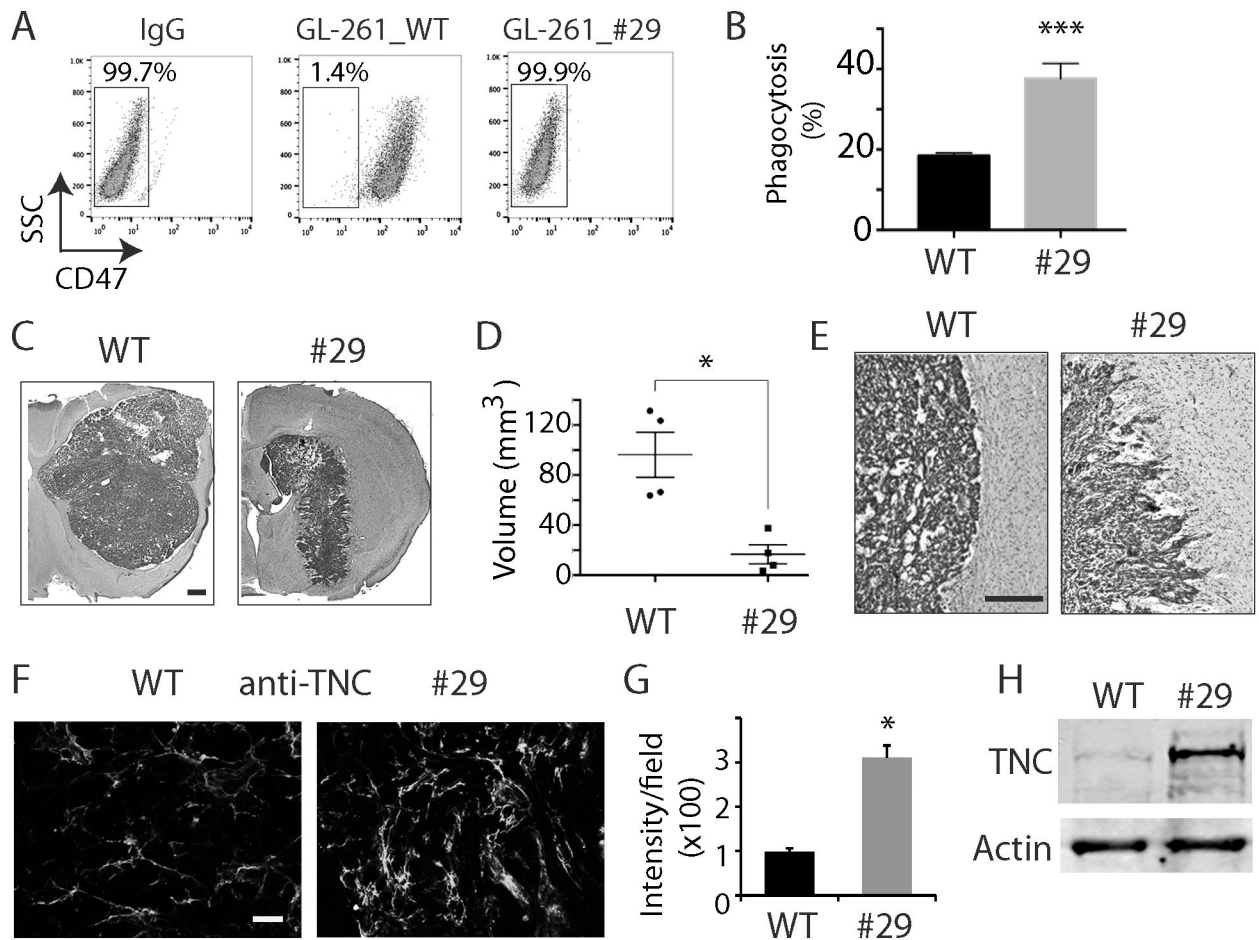
Fig 5. CD47 KO increased TNC expression in immunocompetent mouse models.
A. Flow cytometry analysis with an anti-mouse CD47 antibody indicated no CD47 expression on cell membrane in Cd47$^{-/-}$ cells. **B.** Phagocytosis analysis of THP-1 cells co-cultured with GL261 Cd47 WT and Cd47$^{-/-}$ cells. **C, D.** Representative H &E staining of tumors derived from GL261 cells grown in syngeneic immunocompetent mice C56BL/6. Bar = 500 μm. **E.** H&E staining of well-demarcated margins in WT tumors (left) and irregular Cd47$^{-/-}$ tumor margins (right) in immunocompetent mice. Bar = 100 μm. **F.** Immunostaining showed TNC was upregulated in Cd47$^{-/-}$ tumor. Bar = 100 μm. **G.** Quantification of intensity of TNC in GL261 tumors. **H.** Western blot analysis confirmed that TNC was upregulated in CD47 KO GL261 cells. *: $P<0.05$; ***: $P<0.001$, n=4.
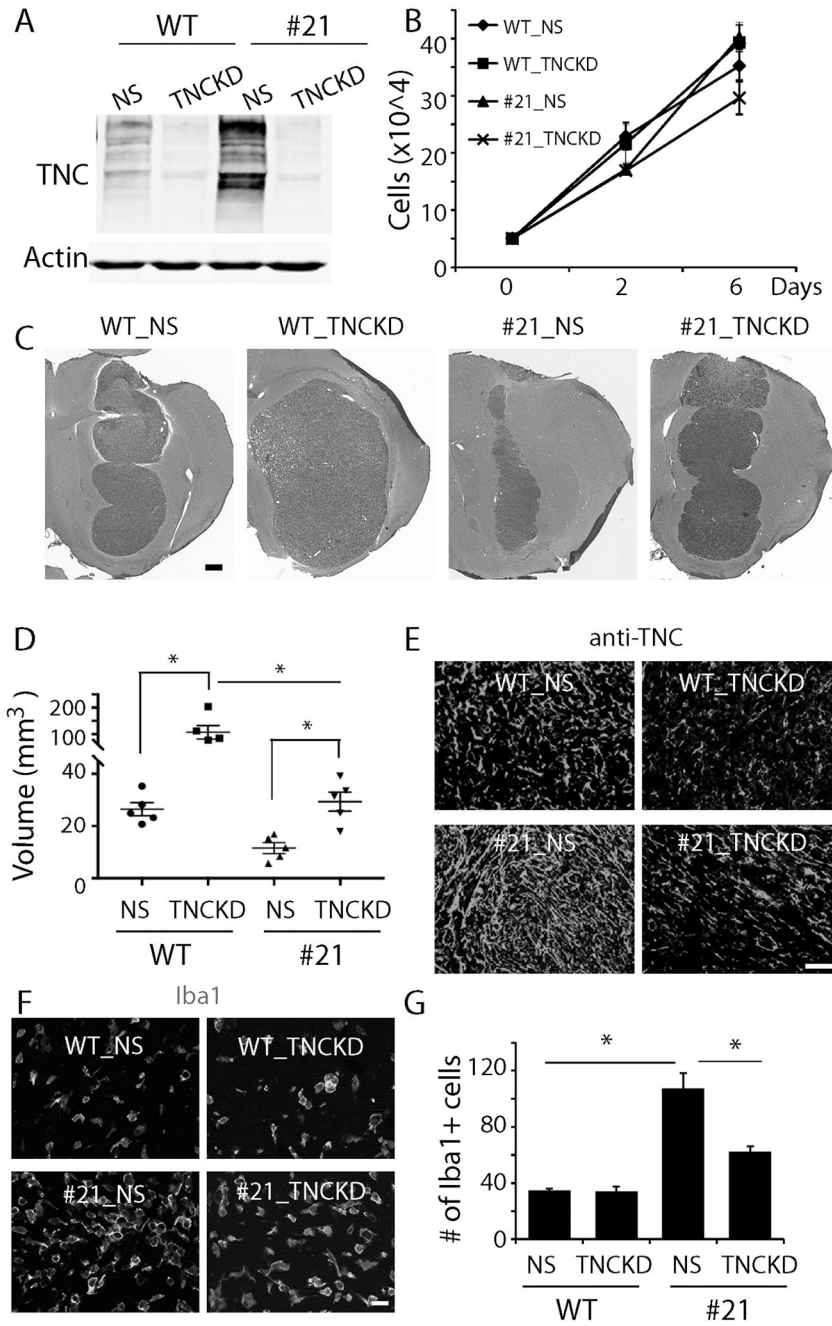
Fig. 6. The effect of TNC loss-of-function on the anti-tumor function of CD47 KO.
A. Knocking down TNC expression in WT cells and clone 21 CD47$^{-/-}$ cells using TNC specific shRNA (TNCKD). Non-silencing shRNA (NS) was used as a control. **B.** Growth curve of TNCKD cells in comparison to their counterparts. **C.** H&E staining of xenografts derived from CD47 WT and CD47$^{-/-}$ cells harboring TNCKD. Bar = 500 μm. **D.** Quantification of tumor size. **E.** Staining of human specific TNC confirmed TNC downregulation in xenografts derived from cells receiving TNC shRNA. Bar = 100 μm. **F.** Staining of the microglial/macrophage marker Iba-1 in TNCKD xenografts. Bar = 20 μm. **G.**

Quantification of the number of Iba-1$^+$ cells in control and CD47$^{-/-}$ xenografts with and without TNCKD. TNCKD decreased Iba1$^+$ cells in CD47$^{-/-}$ xenografts. *: P<0.05, n=5.
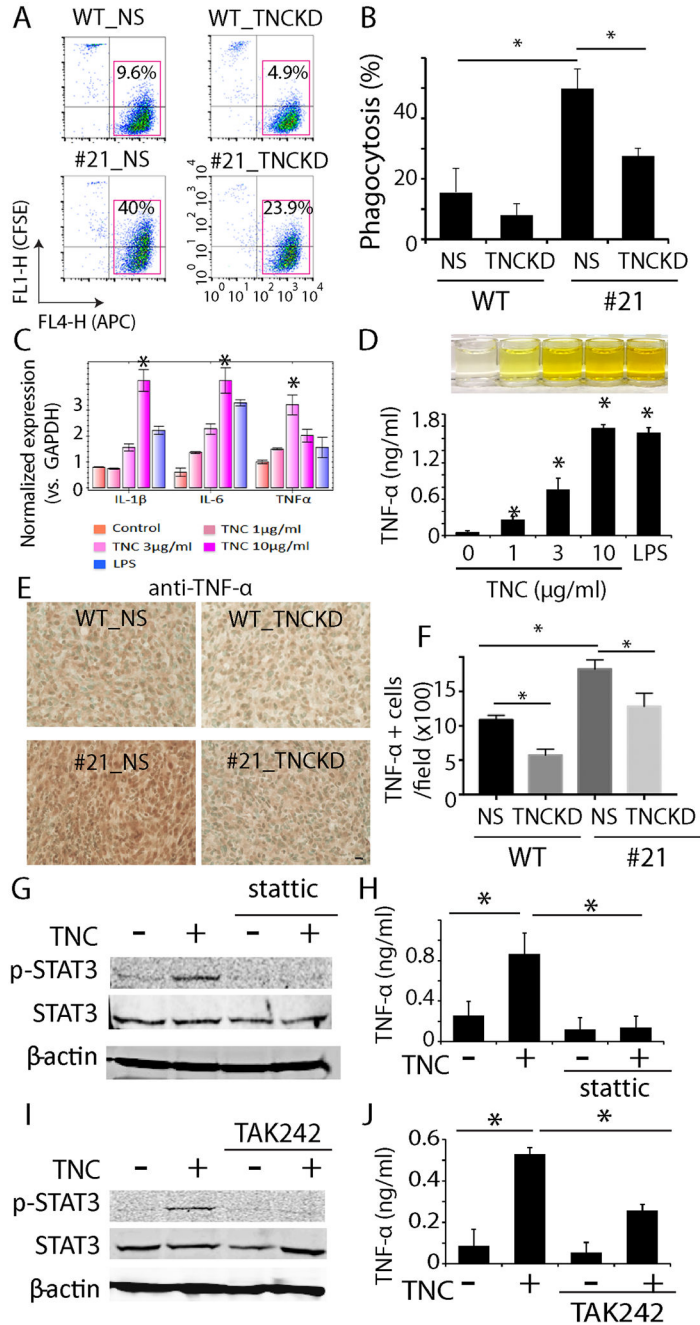
Fig. 7. Effect of TNC on phagocytosis and macrophage cells.
A. TNCKD in tumor cells decreased phagocytosis of WT and CD47$^{-/-}$ cells by
macrophages. **B.** Quantification of phagocytosis, n=3. **C.** RT-PCR indicated that exogenous
TNC induced expression of pro-inflammatory genes including IL-1β, IL-6 and TNF-α in
THP-1 cells in a dose dependent manner. LPS was used as a positive control, n=6. **D.** ELISA
showed TNC increased TNF-α secretion in THP-1 cells in a dose dependent manner, n=3.
E. Immunohistochemistry staining of TNF-α in CD47 WT +/− NS and CD47$^{-/-}$ +/−
TNCKD xenografts. Methyl green (green) was used to counterstain nuclei. Bar = 20 μm. **F.**
Quantification of % of cells with TNF-α staining in the xenografts. n=5. **G.** Immunoblot

analysis indicated that TNC treatment activated STAT3 in THP-1 cells, which was blocked by the STAT3 inhibitor stattic. **H.** Stattic prevented TNF-α production in THP-1 cells treated with TNC, n=3. **I.** TLR4 inhibitor TAK242 blocked STAT3 activation in THP-1 cells in response to TNC. **J.** TAK242 decreased TNC-induced TNF-α production in THP-1 cells, n=3. *: *P*<0.05.